Check for updates

ADVANCED MATERIALS TECHNOLOGIES
www.advmattechnol.de

Fully Printed 3D-Thermoformed Electroluminescent Capacitive System for Human–Machine Interface Applications

Lia Campos-Arias, Nikola Peřinka, Javier Vicente, Vitor Manuel Gomes Correia, Cristian Mendes-Felipe, José Luis Vilas-Vilela, and Senentxu Lanceros-Méndez*

In-mold electronics (IME) has emerged as a suitable approach to enable conformable electronics with improved integration and reduction of assembling parts. It also presents a lower environmental impact comparing with conventional electronics since it requires less material an energy during fabrication. The combination of screen-printing and thermoforming to develop IME products has been used to manufacture sensors and conductive circuits. However, it has not been explored in more complex fields combining several functionalities, such as lighting and sensing. In this work, an electroluminescent capacitive interface by screen-printing and thermoforming is developed. The morphology and electrical properties are analyzed before and after thermoforming to determine the impact of the fabrication process. It is found that the luminance of the thermoformed device is superior to the device before thermoforming. Moreover, the capacitance activity is also tested, obtaining a functional system by combining the sensing capacitance of one of the electrodes and the luminance of another one. To the best of the authors' knowledge, a completely functional screen-printed and thermoformed device with electroluminescent activity and capacitive sensors is reported for the first time. Thus, this work strongly contributes to a broader understanding and application of IME technology.

1. Introduction

The constantly increasing demand for improved integration and conformability of components for electronic devices has led to the development of fabrication methods where electronics and structural parts do not need to be assembled. This is the case of 3D printed electronics,[1] where different layers of functional material are fabricated in its final shape, and in-mold electronics (IME),[2] where functional material are deposited by 2D printing onto a thermoplastic substrate and subjected to thermoforming to obtain the final 3D shape.[3] The automotive industry has boosted the development of IME products, especially human–machine interfaces (HMI), that are undergoing a significant transformation driven by the desire for seamless integration and intuitive user experience.[2,4–6]

One of the limiting factors in the development of HMI is the incompatibility between soft, curvilinear human bodies and the rigid planar electronics.[7] IME is capable of implementing flexible and stretchable electronics into 3D arbitrarily shaped surfaces.[8] However, indium-tin-oxide (ITO) used conventionally as transparent conductors for electronics is not compatible with this technique due to its fragility and rigidity. Furthermore, it presents high cost, and a complex and environmentally unfriendly

L. Campos-Arias, N. Peřinka, J. Vicente, C. Mendes-Felipe, J. L. Vilas-Vilela, S. Lanceros-Méndez
BCMaterials
Basque Center for Materials
Applications and Nanostructures
UPV/EHU Science Park, Leioa 48940, Spain
E-mail: lia.campos@bcmaterials.net

V. M. Gomes Correia
Centre for MicroElectroMechanics Systems (CMEMS)
University of Minho
Campus de Azurém
Guimarães 4800-058, Portugal

V. M. Gomes Correia
Faculty of Engineering
University of Porto
FEUP
Porto 4200-465, Portugal

J. L. Vilas-Vilela
Grupo de Química Macromolecular (LABQUIMAC) Dpto. Química-Física
Facultad de Ciencia y Tecnología
Universidad del País Vasco (UPV/EHU)
Bizkaia, Leioa 48940, Spain

S. Lanceros-Méndez
IKERBASQUE
Basque Foundation for Science
Bilbao 48009, Spain

S. Lanceros-Méndez
Physics Centre of Minho and Porto Universities (CF-UM-UP), and
Laboratory of Physics for Materials and Emergent Technologies
LapMET University of Minho
Braga 4710-057, Portugal

The ORCID identification number(s) for the author(s) of this article can be found under https://doi.org/10.1002/admt.202402116

DOI: 10.1002/admt.202402116

 © 2025 Wiley-VCH GmbH

fabrication process. To substitute it, silver nanowires or poly(3,4-ethylenedioxythiophene) polystyrene sulfonate (PEDOT:PSS) are some of the options, since they present flexibility and stretchability as well as suitable electrical conductivity.[7,9,10]

IME technology allows the increase in design flexibility and simplification of the manufacturing process by reducing the number of fabrication steps, resulting in a reduction in raw material use, production time and costs, with the elimination of additional assembly and handling step,[11] automating the process easily. Moreover, the conventional surface mounted rigid components are restricted to be located in low deformation parts. Their substitution by printed electronic components may improve the durability of the device by increasing the mechanical integrity of the products.[12–14] Therefore, not only material consumption and assembly labor will be reduced, but also it will be translated into a lower environmental impact, reducing waste and energy consumption during manufacturing.[11,12,15–17]

There are few studies of combined printing and thermoforming to fabricate IME products, although the combination has a great potential. Among printing methods, screen-printing is fast, simple and efficient, it can work under normal environmental conditions and is affordable and scalable.[18,19] On the other hand, thermoforming has been extensively used in product packaging for diverse applications (medicines, food, and medical equipment), therefore, it is a well-known technique.[20] Materials subjected to thermoforming must stand temperatures of 120–200 °C[3] and tolerate large strain under processing conditions so they need to be flexible and stretchable to be 3D permanently shaped.[2,21] These two methods have been used to fabricate sensors[6] or conductive circuits,[22] but there is a lack of conformable lighting applications, which can be also combined with sensing capabilities.

One of the main methods used currently in displays and lighting technology is alternative current electroluminescence (ACEL). This phenomenon was discovered by Destriau in 1935, when he suspended copper doped zinc sulfide (ZnS:Cu, phosphor powders) in castor oil and insulated it from two electrodes with mica sheets.[23] When a high AC voltage is applied, a light emission is observed, explained by the following phenomena: electron injection, electron transport, impact excitation and radiative recombination with optical outcoupling. The application of a high AC voltage generates a high electric field in the phosphor layer that causes, at the same time, the injection by tunneling emission of the electrons trapped at the insulator-phosphor interface into the phosphor layer. These injected electrons are accelerated and transported through the phosphor layer, impacting and exciting luminance centers (impurities) in the layer. When those excited luminance centers return to their ground states, the excess energy is released in the form of photon emission.[24] In **Figure 1**, it is illustrated the structure of an ACEL device and the corresponding equivalent circuit.

Comparing with light emitting diodes (LEDs), the other leading technology in lighting and displays electronics, ACEL devices present several advantages. While LEDs are point light sources, ACEL devices are surface light sources with uniform emission that can be obtained in a very thin structure, allowing the fabrication of flexible devices and wide area lighting. The manufacturing process is simple and can be performed in an ambient environment enabling the use of low-cost printing methods such as

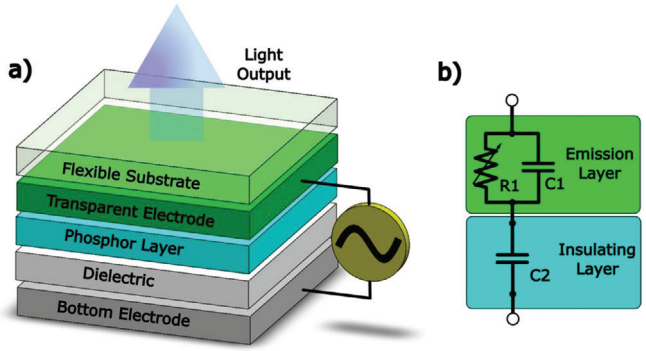


Figure 1. a) Schematic illustration of an ACEL device and b) its equivalent circuit.

screen-printing.[25–27] Moreover, unlike LEDs, ACEL devices are very robust, and they can work between −60 and 95 °C. Finally, even though ACEL devices need high voltage to work (>100 V), they require very low current densities and consequently they operate at low powers. Among their drawbacks, it should be mentioned their limited color capabilities, i.e., a single material emits light in a narrow wavelength so they need color conversion layers. Further, high levels of humidity can cause reduction in brightness and they present low lumen output performances.[24] Nonetheless, their luminance is usually enough for low-cost lighting and large area display applications.[28]

In this study, we have developed an electroluminescent capacitive interface fabricated by screen-printing and conformed to a 3D shape by thermoforming. The morphology and electrical properties of the device were characterized and the electroluminescent performance was analyzed before and after thermoforming. The capacitive sensors performance was also evaluated. To the best of our knowledge it is the first report of a functional screen-printed and thermoformed device with electroluminescent activity and capacitive sensors. Therefore, this work contributes to a broader understanding and applicability of the IME technology.

2. Experimental Section

2.1. Materials

Resin Rigid 10K (tensile modulus: 10.0 GPa, elongation at break: 1%, heat deflection temperature at 0.45 MPa: 163 °C) was purchased from Formlabs, USA. Polyethylene terephthalate glycol (PETG) substrate (33 × 25 cm, 0.5 mm thickness, 72 °C heat distortion temperature at 0.455 MPa, glass transition 79–80 °C) was purchased from Machines-3D, France. Transparent Ink Orgacon EL-P3165 (PEDOT:PSS-based ink, solid content: 2.5 wt%, recommended curing temperature: 120–130 °C for 2–3 minutes (minimum 80 °C), viscosity: >25 Pa s, sheet resistance at P120: 375–425 Ω sq^{-1}, sheet resistance × optical density (ASTM D 1003): 11) was purchased from AGFA, Belgium. Thermoset White Phosphor Paste C2180612D1 (zinc sulfide doped predominantly with copper-based ink, solid content: 78.5%–82.5%, recommended drying temperature: 130 °C for 10 min, viscosity (Haake RS1 C20/2°TiL 230 s^{-1} at 25 °C): 0.9–2.5 Pa s, luminance (photoluminescence): 29.2 cd m^{-2}) was purchased from

© 2025 Wiley-VCH GmbH

2365709x, 2025, 11, Downloaded from https://advanced.onlinelibrary.wiley.com/doi/10.1002/admt.202402116 by Universidade Do Minho, Wiley Online Library on [27/04/2026]. See the Terms and Conditions (https://onlinelibrary.wiley.com/terms-and-conditions) on Wiley Online Library for rules of use; OA articles are governed by the applicable Creative Commons License

SunChemical, UK. Crossover dielectric ME779 (solid content: 65%–67%, recommended drying temperature: 120 °C for 20 min, viscosity (Brookfield RVT #14 spindle, 10 RPM, 25 °C): 50–70 Pa s, dielectric constant (κ): 18, breakdown voltage (1 mm traces at 90° with ≥25 µm dielectric): >2.5 kV) and Silver Paste ME603 (solid content: 53.5%–57%, recommended drying temperature: 120 °C for 20 min, viscosity (Brookfield 0.5 x RVT, #14 spindle, 10 RPM, 25 °C): 25–50 Pa s, resistivity: ≤35 mΩ sq^{-1} mil, resistivity after thermoforming (it can vary depending on the degree of elongation): ≤300 mΩ sq^{-1} mil) were purchased from DuPont Ltd., UK.

2.2. Mold Design

The mold for thermoforming was designed by Autodesk Inventor 3D modeling graphic software, with the final model converted to the STEP format, and fabricated using the resin rigid 10K in a 3D printer (Mars 3, ELEGOO) to simulate the shape of a computer mouse. Thus, allowing the device to be demonstrated as a capacitive sensing interface with integrated optical response. The 3D mold is shown in **Figure 2** and the design file is provided as the Supporting Information.

The modeling process was carried out considering the manufacturing method (3D printing) and the requirements of the thermoforming process of the samples, minding the position of the critical elements and bending radius of the conductive layers to avoid excessive deformations for the electrical circuits.

2.3. Screen-Printing and Thermoforming Process

Inks were screen-printed onto the PETG substrate with a semi-automatic screen-printing DX3050P from Shenzhen Dstar Machine Co., using different polyester screen mesh for each ink in the following order: first, one layer of PEDOT:PSS transparent ink (mesh count: 77 wires cm^{-1}, 48 µm wire diameter), second, one layer of phosphor ink (mesh count: 61 wires cm^{-1}, 64 µm wire diameter), third, four layers of dielectric ink (mesh count: 61 wires cm^{-1}, 64 µm wire diameter), and finally, one layer of silver paste (mesh count: 110 wires cm^{-1}, 34 µm wire diameter). Each individual layer was cured in an oven (J.P. Selecta, Digitronic-TFT) at 60 °C for 1 h. Dielectric layers were cured 10 min between each layer and then finally cured for 1 h.

After the layers were dried, the sample was subjected to thermoforming on a Vaquform DT2 with the mold previously fabricated. Set point temperature was 130 °C and parameters k (related with the cooling time of the forming cycle) and v (control of the air flow and pressure of the vacuum system) were set to 1 and 0, respectively. Figure 2 shows the different layers and a scheme of the mold for thermoforming process.

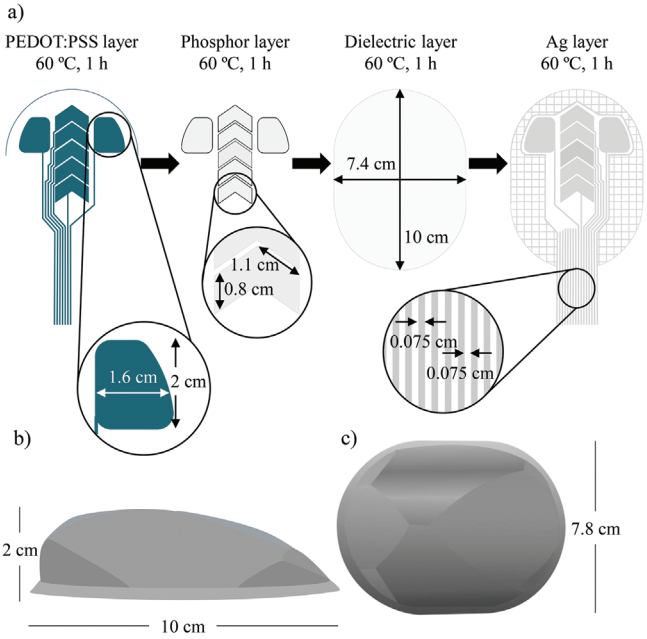


Figure 2. Illustration of the a) screen-printing process and the b) lateral view and c) top view of the mold.

2.4. Characterization Methods

Substrate deformation (ϵ) was studied in order to evaluate how it may affect the printed circuit. For that purpose, a grid was screen-printed onto PETG and distances between lines were measured before and after thermoforming. Deformation was calculated after Equation (1):

$$\epsilon = \frac{d_{TF} - d_i}{d_i} \times 100 \quad (1)$$

where d_{TF} is the distance between consecutive lines after thermoforming and d_i is the distance between the same lines before thermoforming.

To analyze the morphology of the layers before and after thermoforming, a sample of each electrode was cut and immersed in molds with 100% of epoxy resin (Kit Embed 812 from Electron Microscopy Science, EMS #14120) and contained at 60 °C in the oven for 48 h to allow the resin to cure. Then, to cut the samples, a Leica UCT Ultramicrotome was used, and the electrodes' layers were analyzed in cross-section with a scanning electron microscope (Hitachi S-3400) at an acceleration voltage of 15 kV. Prior to introducing the samples in the microscope, all of them were metallized (Leica ACE 200) by sputtering with 5 nm gold.

The electrical properties of the device before and after thermoforming were analyzed. First, resistance of Ag and PEDOT:PSS layers, screen-printed separately, was measured by a two-point probe multimeter (Amprobe AM-510-EUR) from the connector terminal to the electrode. Then, dielectric measurements of the complete stacks were carried out at room temperature in the 100 Hz to 1 MHz frequency range using a Precision *LCR* Meter (E4980A, 20 Hz to 2 MHz, Keysight) connected to the specific component to be characterized by two-point probes. The following parameters were obtained: parallel capacitance (C_p) and parallel resistance (R_p) for the capacitors.

2.5. Electroluminescent Measurements

To evaluate the optoelectronic response of the devices before and after the thermoforming process, electroluminescent

© 2025 Wiley-VCH GmbH

2365709x, 2025, 11, Downloaded from https://advanced.onlinelibrary.wiley.com/doi/10.1002/admt.202402116 by Universidade Do Minho, Wiley Online Library on [27/04/2026]. See the Terms and Conditions (https://onlinelibrary.wiley.com/terms-and-conditions) on Wiley Online Library for rules of use; OA articles are governed by the applicable Creative Commons License

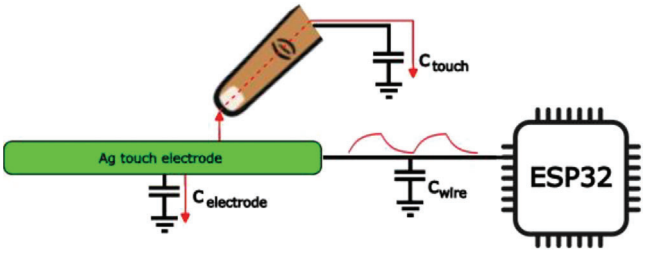


Figure 3. Architecture of the capacitive detection system based on the ESP32-S3 MCU: demonstrative scheme of the methods of self-capacitive detection.

measurements were performed by fiber-optic spectrometer AvaSpec-ULS2048CL-EVO connected to fiber-optic cable FCR-7UVIR200-2-ME and a cosine corrector (CC-VIS/NIR, 3.9 mm active area,18 mm (L) × 6.5 mm (OD) to collect light from a 180° angle) from Avantes. The devices were powered by a variable voltage AC power supply (PCR1000WE, Kikusui). Measurements were carried out at different frequencies (100–1000 Hz, in 100 Hz intervals), keeping the voltage constant at 120 V, and at different voltages (40–220 V, in 20 V intervals), while keeping the frequency at 400 and 1000 Hz. Every electrode was measured in three spots before and after thermoforming and the obtained values are the average of them.

For the evaluation of the luminous efficacy, an electrical characterization was performed using the AC power supply and a multimeter (Keithley 2110) connected in series with the electrodes to measure the electrical AC current. The electrodes were tested before and after thermoforming with the same conditions of the electroluminescent measurements (from 100 to 1000 Hz in 100 Hz intervals at 120 V, and from 40 to 220 V in 20 V intervals at 400 and 1000 Hz).

2.6. Evaluation of the Prototype

2.6.1. Capacitive Interface Analysis

The technology developed for touch detection is based on the analysis of the variation of the capacitive coupling in self-capacitance mode. This variation was generated between a conductive material, such as a finger, and the electrodes. For capacitive sensing, each electrode was connected to an ESP32 microcontroller (MCU) (ESP32-S3-WROOM-2-N32R8 V) capacitive sensing input. The architecture of the detection system can be divided into three basic blocks: conductive electrodes for detection, signal processing (within the IC), and MCU/application, as shown in **Figure 3**.

The capacitance of the circuit increases when a human finger approaches, adding another capacitor to the system. This additional capacitor affects the charge and discharge times of the circuit and increases the overall capacitance of the circuit. Thus, the user's contacts will be indicated by a variation in the duration of the charge–discharge along the circuit. When this value deviates from the default, the microcontroller notifies the main controller that the user has carried out an interaction with the circuit.

ESP32 MCU was selected considering the previous electrical characterization of the devices and the deformation that the electrodes will suffer after thermoforming.

2.6.2. Electroluminescent Interface Analysis

In a simplistic way ACEL devices resemble a parallel plate capacitor (Figure 1b) which is often called a "leaky condenser." The ACEL device can, therefore, be modeled with the standard circuit diagram of capacitor and resistors, considering the capacitor discharge.[29] The performance of the device was evaluated to demonstrate the potential of this technology for HMI applications, specifically as a computer mouse prototype. Thus, the thermoformed circuit was connected to the electronic circuit shown in Figure S1 (Supporting Information). This allowed to evaluate the performance in activating the electroluminescent zones and capacitive touch detection, focusing on the luminous intensity, electrical consumption, and touch detection response.

3. Results and Discussion

3.1. Analysis of the Thermoforming Process

In **Figure 4** is represented the mold, the device thermoformed and the deformation color map of the substrate with the screen-printed grid. It is observed that the deformation of longitudinal (c) and transversal (d) lines is at its maximum in the borders of the mold, as expected (88% elongation and 27% shrinkage for longitudinal lines, 68% elongation and 33% shrinkage for transversal lines). Longitudinal lines stretch where transversal lines shrink and vice versa, as can be seen in the color maps (magenta is for stretching zones, blue-purple for shrinking zones) in Figure 4c,d. Moreover, as elongation of the longitudinal lines in the left side is larger than in the right side, the silver and PEDOT:PSS conductive traces are better located on right side of the device, as can be observed in Figure 4b. On top of the mold, the deformation is minimum. Thus, the design of the mold seems suitable for thermoforming the screen-printed device without damaging the structure and reducing functionality.

Figure 5 shows an image of the system before and after thermoforming as well as an image of the thermoformed device with an overlap of the electrodes prior to thermoform. Each electrode is connected to the connector through a 0.75 mm wide conductor (Ag layer). It should be noted that, considering the fragility of the PEDOT:PSS layer, an Ag layer was deposited as an interface between this layer and the electrical connector (Figure 5), thereby ensuring greater stability of the electrical signal and adequate mechanical reinforcement of the PEDOT:PSS layer.

The lateral electrodes corresponding to EL1 and EL2 present a total area per electrode of 283.59 mm^2 while EL3–EL7 show a total area of 154.78 mm^2 per electrode. The thermoformed sample presented an increase of ≈25% in the area of the electrodes comparing with the 2D (overlapped green) sample. Therefore, a variation in the capacitance of the electrodes occurs due to thermoforming process.

© 2025 Wiley-VCH GmbH

2365709x, 2025, 11, Downloaded from https://advanced.onlinelibrary.wiley.com/doi/10.1002/admt.202402116 by Universidade Do Minho, Wiley Online Library on [27/04/2026]. See the Terms and Conditions (https://onlinelibrary.wiley.com/terms-and-conditions) on Wiley Online Library for rules of use; OA articles are governed by the applicable Creative Commons License

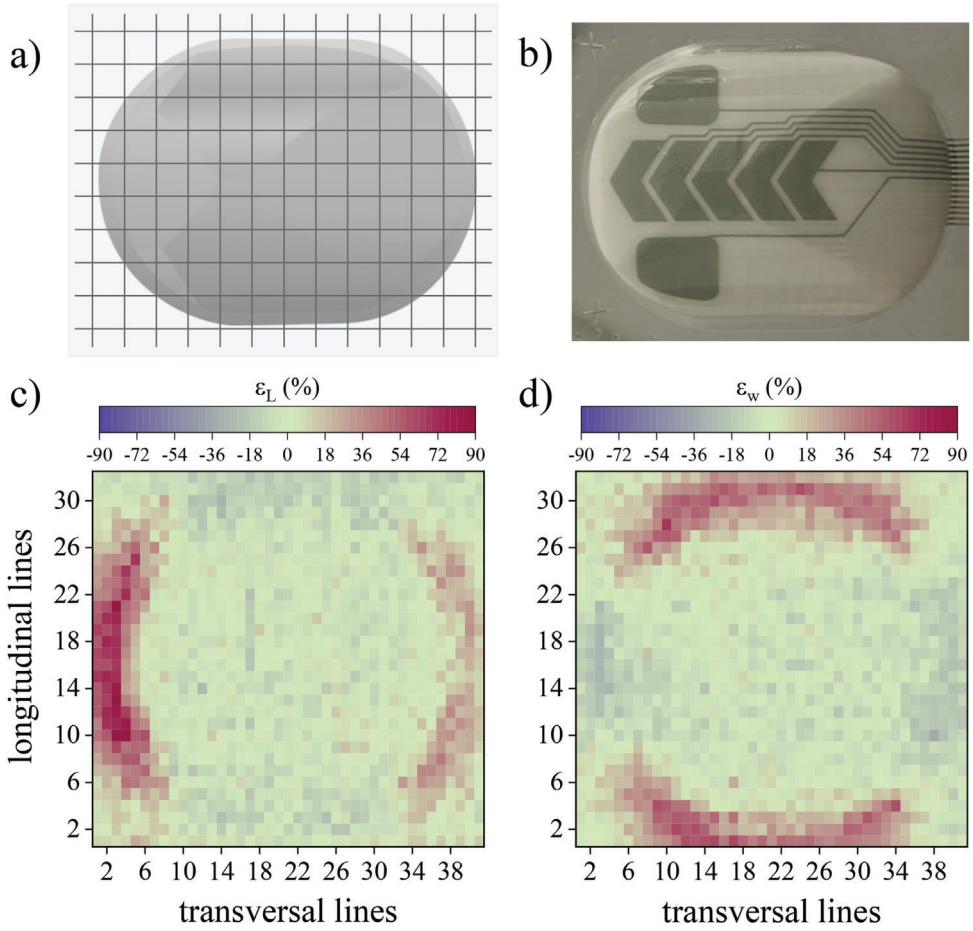


Figure 4. Representation of the mold with the a) screen-printed grid and b) thermoformed device from the top view. Color map of the substrate deformation: elongation of the c) longitudinal and d) transversal lines printed on the PETG substrate.

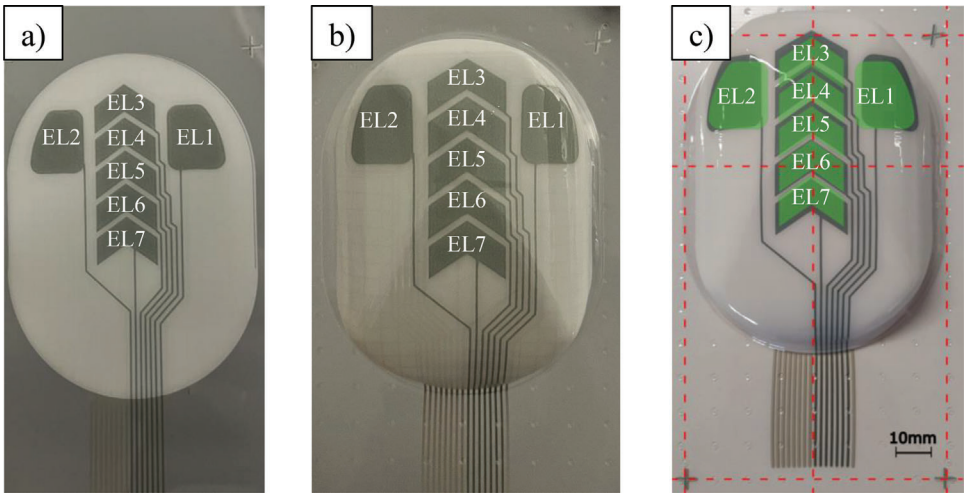


Figure 5. Sample a) before and b) after thermoforming and analysis of the variation of the c) electrodes surface area in the thermoformed device in relation to the electrodes (green) without thermoforming.

© 2025 Wiley-VCH GmbH

2365709x, 2025, 11, Downloaded from https://advanced.onlinelibrary.wiley.com/doi/10.1002/admt.202402116 by Universidade Do Minho, Wiley Online Library on [27/04/2026]. See the Terms and Conditions (https://onlinelibrary.wiley.com/terms-and-conditions) on Wiley Online Library for rules of use; OA articles are governed by the applicable Creative Commons License

3.2. Morphological and Electrical Properties of the Printed Electrodes

Representative SEM images of the electrode cross-section are depicted in **Figure 6** as well as the corresponding layer thickness. Three layers printed on the substrate can be observed: the phosphor, the dielectric and the silver layer. PEDOT:PSS transparent layer cannot be observed in the images (≈1 µm thickness). Each layer of the non-thermoformed (a and d) and thermoformed samples (b, c, e, f, g, h, and i), presents similar morphology. In the phosphor layer, an inhomogeneous distribution of subangular particles (ZnS doped with Cu) with similar sizes (≈10–33 µm of diameter) can be observed, bound by the thermoset resin, with no relevant voids or pores. The thickness of this layer is in the range of 26–35 µm for all the samples. Above the phosphor layer, dielectric layer can be observed, which presents a smooth surface with thickness in the range of 30–39 µm. This layer is infiltrated in the phosphor layer due to the irregularity of the latter layer but it shows a flat surface to deposit the silver layer on top. Finally, the silver layer is the thinnest one (5–7.5 µm) and it is composed of nanometric silver particles as observed in the images. It is worth mentioning that none of the layers are notably thinner in the thermoformed samples, in fact, comparing the thickness of the complete stack before and after thermoforming, it is shown in Figure 6k that the thermoformed stack is 4%–11% thinner (≈76 µm thickness for electrodes without thermoforming (a, d) versus 68–73 µm for thermoformed electrodes (b, c, e, f, g, h, i)). Moreover, comparing thermoformed and non-thermoformed samples, there are no significative differences in thickness variation between EL1–EL2 and EL3–EL7 even though EL1–EL2 are in the lateral sides where deformation is more pronounced. The similarity in mechanical properties of the different layers promotes homogeneity and minimizes the risk of interlayer delamination, which has not been observed in the SEM images.

Electrical resistance of Ag and PEDOT:PSS traces before and after thermoforming is displayed in **Figure 7**. It is observed that resistance measurements of Ag traces (a) are lower after thermoforming, while PEDOT:PSS traces (b) show an increase in electrical resistance after thermoforming. The different behavior of Ag and PEDOT:PSS layers toward thermoforming is caused by opposite mechanisms during the process: on the one hand, elongation causes particle separation while, on the other hand, heat and pressure induce particle compression; consequently, the former effect triggers an increment in electrical resistance while the latter leads to a reduction in this property.[30] It is possible to observe the offset of the first effect over the second one in PEDOT:PSS resistance measurements, while the second effect prevails over the first one in the case of Ag values. The prevalence of one effect over the other arises from the distinct morphologies of the inks. Ag ink contains particles that partially melt at higher sintering temperature and increase the contact among them more easily than the polymeric chains of PEDOT:PSS, which rather separate from each other by the elongation of the process. Besides, the particle content of Ag ink is 50%–60% while PEDOT:PSS ink presents 2.5 wt% of solid content. Furthermore, the decrease in electrical resistance after thermoforming the Ag layer is more pronounced due to the sintering temperature of the ink. The recommended temperature for sintering Ag ink is 120 °C; however, the substrate glass transition (T_g) is 79–80 °C. Heating the sample above the T_g will trigger the deformation of the substrate and will hinder the subsequent thermoforming. Thus, it was necessary to sinter the ink below the optimal temperature, consequently leading to higher resistance values. In the case of PEDOT:PSS layer, the minimum sintering temperature (80 °C) is closer to the experimental sintering temperature (60 °C) so the curing process was completed before thermoforming.

Apparently, none of the silver traces present any discontinuity on the line, so the difference in resistance between electrodes must be due to some artifacts during printing (i.e., the squeegee may apply more pressure in one side of the screen, the ink may not be equally distributed or some holes may be clogged). In the case of PEDOT:PSS, the tendency ($R_{EL7} < R_{EL6} < R_{EL5} < R_{EL4} < R_{EL3}$) is attributed to the difference in the length of the traces. To further mitigate variations in electrode conductivity, adjustments could be made by modifying the electrode design with respect to the printing direction and the width of the traces to compensate length differences.

Most of the electrically conductive inks for in-mold electronics available in the market are based on silver flakes and elastomeric components,[31] as the one used in this work. In order to further explore other alternatives for the bottom electrode, the silver layer can be substituted by silver-coated-copper-based inks. This type of ink has been evaluated[3] and has been proven to endure thermoforming processes, be more air stable than bare copper and maintain high electrical conductivity thanks to the silver coating. Moreover, this change of ink, would also be beneficial to reduce the costs of the devices, associated to the use of silver.

Figure 8a shows the impedance spectroscopy of EL1 for frequencies ranging from 100 Hz to 1 MHz, both before and after thermoforming. The impedance is represented by parallel capacitance and resistance, corresponding to the parallel equivalent circuit model commonly used for measuring high-impedance samples. The electrodes display typical high dielectric loss impedance behavior for polymeric materials, with a significant reduction in permittivity observed between 1 and 10 kHz due to dielectric relaxation. Consequently, a sharp decrease in electroluminescence would be expected for frequencies higher than 2 kHz.

After thermoforming, the parallel capacitance increases, while the parallel resistance decreases. These changes can be attributed to geometric modifications of the electrodes, as capacitance is directly proportional to the surface area of the electrodes, whereas resistance is inversely proportional to it.

The measured impedance for the electrodes EL2–EL7, before and after thermoforming, are shown in Figure S2 (Supporting Information).

The capacitance formed between PEDOT:PSS and Ag layers at 1000 Hz for each electrode before and after thermoforming is displayed in Figure 8b. These values were compared with the values obtained from the theoretical characteristics of the inks, calculated by applying the simplified equation to determine the capacitance (C) of parallel plate capacitors:

$$C = \kappa \cdot \varepsilon_0 \cdot \frac{A}{d} \tag{2}$$

where κ is the dielectric constant of the material, A is the overlapping surface areas of the plates in m^2, d is the distance between the plates in m, and ϵ_0 is the vacuum permittivity. The

© 2025 Wiley-VCH GmbH

2365709x, 2025, 11, Downloaded from https://advanced.onlinelibrary.wiley.com/doi/10.1002/admt.202402116 by Universidade Do Minho, Wiley Online Library on [27/04/2026]. See the Terms and Conditions (https://onlinelibrary.wiley.com/terms-and-conditions) on Wiley Online Library for rules of use; OA articles are governed by the applicable Creative Commons License

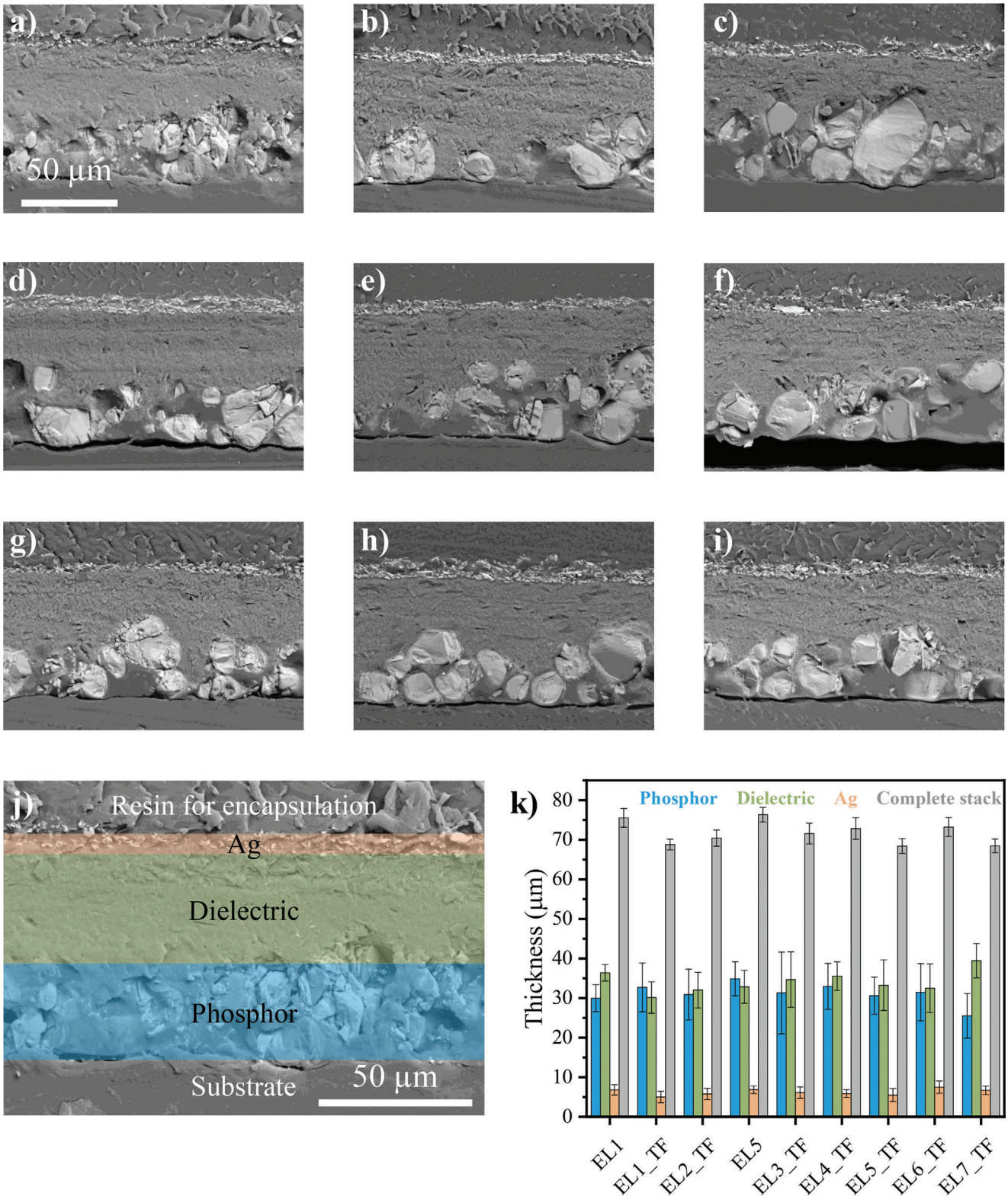


Figure 6. Cross-section SEM images of the electrodes and layers thickness. a) EL1 (the scale bar applies for images a–i), b) EL1_TF, c) EL2_TF, d) EL5, e) EL3_TF, f) EL4_TF, g) EL5_TF, h) EL6_TF, i) EL7_TF, j) layers differentiated by colors and k) bar graph with the thickness of the different electrodes.

© 2025 Wiley-VCH GmbH

2365709x, 2025, 11, Downloaded from https://advanced.onlinelibrary.wiley.com/doi/10.1002/admt.202402116 by Universidade Do Minho, Wiley Online Library on [27/04/2026]. See the Terms and Conditions (https://onlinelibrary.wiley.com/terms-and-conditions) on Wiley Online Library for rules of use; OA articles are governed by the applicable Creative Commons License

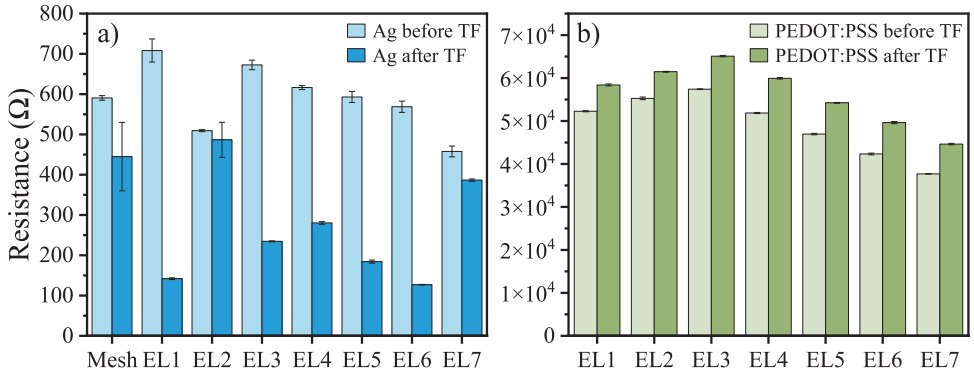


Figure 7. Electrical resistance before and after thermoforming of a) Ag traces and b) PEDOT:PSS traces.

difference between theoretical and experimental values is low in both cases (before and after thermoforming) as well as the variation between electrodes, showing the stability and quality of the process.

3.3. Electroluminescent Measurements

Electroluminescent results of EL1 and images of the device before and after thermoforming are displayed in **Figure 9**. Their spectra collected at different voltages and frequencies are presented in **Figure 10**. The electroluminescent results for the electrodes EL2–EL7 (Figures S3–S8, Supporting Information), the corresponding spectra (Figures S9–S14, Supporting Information), and a video (Video S1, Supporting Information) of the samples emitting light, before and after thermoforming, are shown in the Supporting Information.

All the electrodes before and after thermoforming show an optical response upon applying a voltage at different frequencies. The light emitted from electrodes of both devices is uniform as extracted from the small standard deviation. Luminance of EL1 after thermoforming was higher than before TF as it can be observed in Figure 9b,c. This was expected, as previously observed in resistance measurements, considering that the thermoforming process has a positive effect on inks sintering. However, other factors, such as better contact flake-like silver particles, changes in surface roughness, or interface optimization during thermoforming, could contribute as well to the luminance improvement. This phenomenon is observed also in the other electrodes (Figures S3–S8, Supporting Information). On average, luminance increased by 16.2% across various testing frequencies after thermoforming. Regarding the voltage applied, the improvement after thermoforming decreases as the voltage increases. Finally, the color space chromaticity diagram (links the visible spectrum of specific colors with the visual sensation of human color vision) of the luminance shows a shift from green toward blue at increasing frequencies and a shift from blue toward white at increasing voltages. The color luminance perception is almost the same for thermoformed and non-thermoformed devices. This color tunability as a function of the voltage or the frequency can be beneficial for the specific applications.

In Figure 10, it can be observed that independently of the applied frequency and voltage, the spectra present two emission bands, in the blue (450–500 nm) and in the intersection of the green and red (≈580 nm, yellow) spectral regions. The bands observed are characteristic of the ZnS:Cu,Cl (450–500 nm) and ZnS:Mn (580 nm),[32,33] showing that the phosphor layer is probably composed of a mixture of ZnS:Cu,Cl particles and ZnS:Mn,

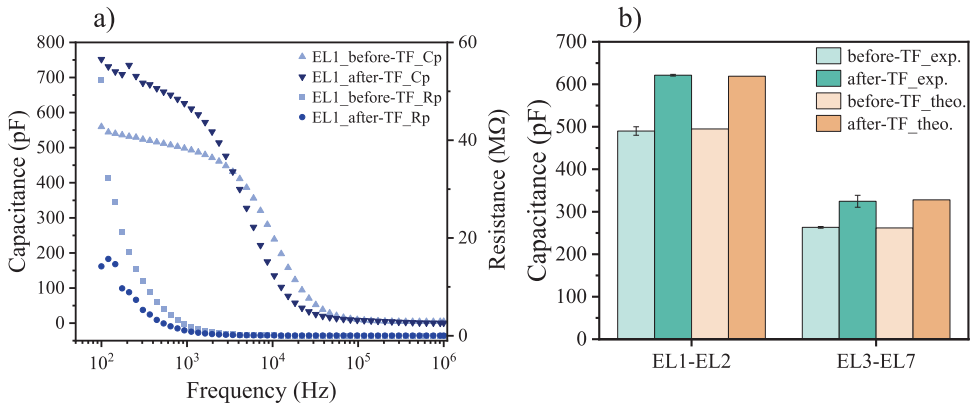


Figure 8. a) Impedance spectroscopy of EL1 and b) experimental (exp.) and theoretical (theo.) capacitance values of the electrodes at 1000 Hz, before and after thermoforming.

© 2025 Wiley-VCH GmbH

2365709x, 2025, 11, Downloaded from https://advanced.onlinelibrary.wiley.com/doi/10.1002/admt.202402116 by Universidade Do Minho, Wiley Online Library on [27/04/2026]. See the Terms and Conditions (https://onlinelibrary.wiley.com/terms-and-conditions) on Wiley Online Library for rules of use; OA articles are governed by the applicable Creative Commons License

2365709x, 2025, 11, Downloaded from https://advanced.onlinelibrary.wiley.com/doi/10.1002/admt.202402116 by Universidade Do Minho, Wiley Online Library on [27/04/2026]. See the Terms and Conditions (https://onlinelibrary.wiley.com/terms-and-conditions) on Wiley Online Library for rules of use; OA articles are governed by the applicable Creative Commons License

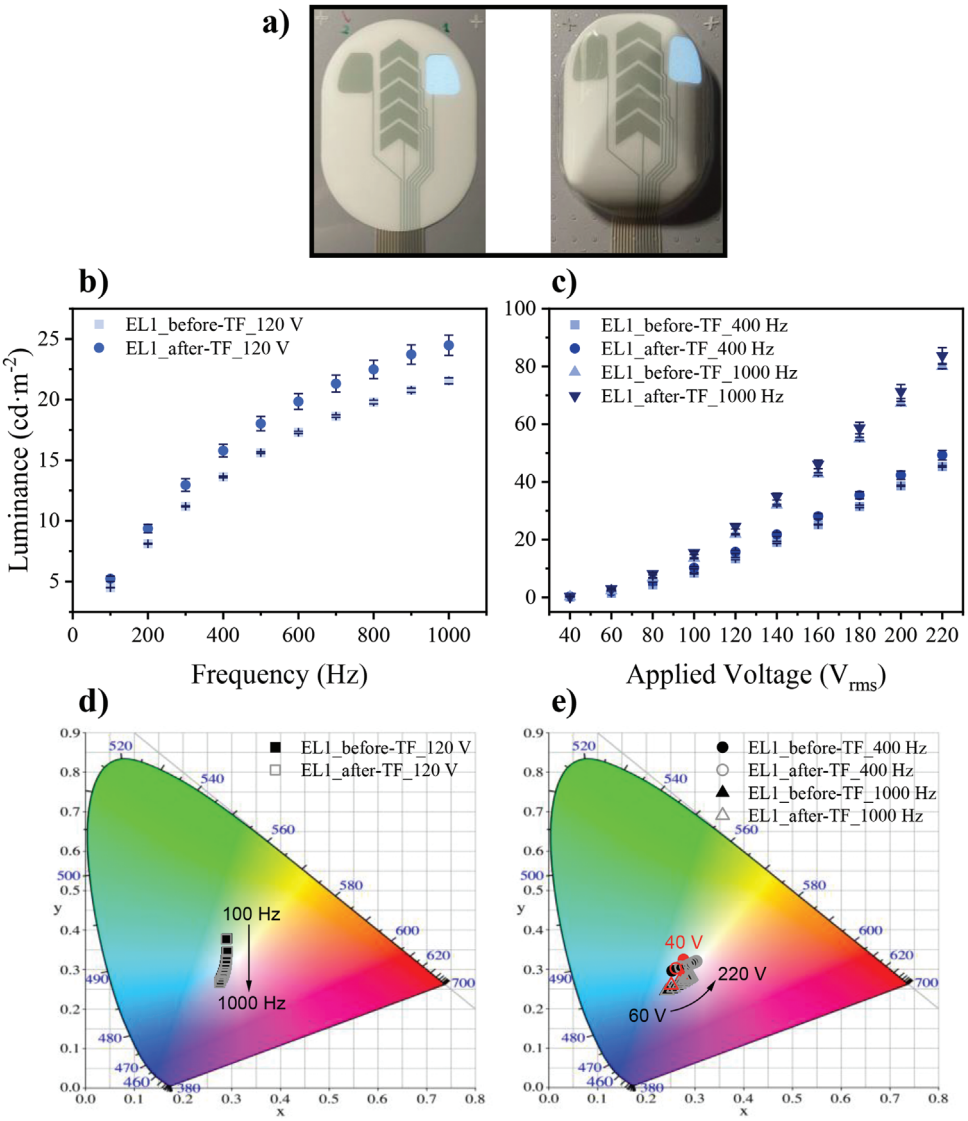


Figure 9. a) Images of devices before and after thermoforming applying 100 V at 400 Hz to EL1. b) Luminance of EL1 at different frequencies, and c) various applied voltages. Color space chromaticity diagram (showing the CIE coordinates (International Commission on Illumination)) for each d) frequency and e) voltage.

being the first ones in major proportion since its band is more intense.

At increasing frequencies (Figure 10, first row), it is noticeable that both bands become narrower. The blue region band is blueshifted from 500 to 450 nm and the yellow region band remains unchanged in wavelength position. This blueshift has been attributed previously to the coexistence of ZnS in cubic and hexagonal form, making the wavelength dependent on the crystallographic site of the impurity.[34,35] Besides, the ratio of intensities corresponding to the blue:yellow region bands changes slightly, decreasing with increasing frequencies until 500 Hz (from 1.42 to 1.22 approximately in both cases before and after thermoforming) and then it increases (to 1.51 in both cases). The reason behind is that high frequencies do not allow enough time for the Mn^{2+} excited electrons to relax and reexcite again, triggering the saturation of the yellow band.[36] This applied for both thermoformed and non-thermoformed devices and is observed in all the electrodes.

It is worth mentioning that despite in literature can be found that the increase in voltage does not change the blue and yellow intensities,[36] in this work a clear change is observed. At 400 Hz (Figure 10, second row), the ratio of intensities corresponding to the blue:yellow region bands decreases as the voltage increases, from 1.67 to 0.99 before thermoforming and from 1.43 to 0.99 after thermoforming. Something similar happened at 1000 Hz (Figure 10, third row); however, the difference is bigger: the ratio blue:yellow reduces from 2.3 to 1.3 before thermoforming and from 2.2 to 1.2 after thermoforming as the voltage increases. In any case, the difference in the ratio of intensities is the cause of perceiving light as white at 400 Hz and slightly blue at 1000 Hz, which agrees with the color space chromaticity diagram. The same characteristics can be observed in EL2–EL7

 © 2025 Wiley-VCH GmbH

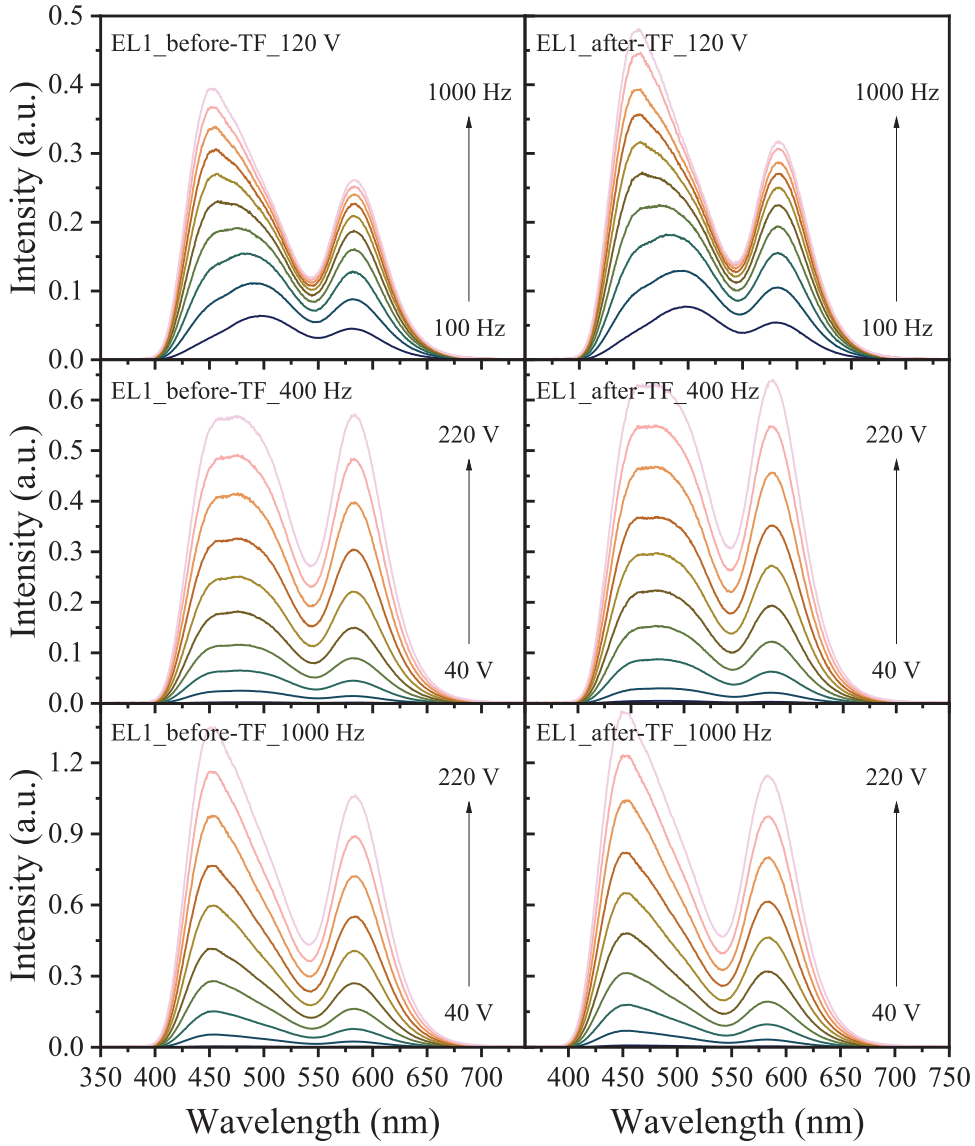


Figure 10. Spectra of EL1 at different frequencies and voltages of the non-thermoformed (left) and the thermoformed (right) device.

(Figures S9–S14, Supporting Information) even though they are printed in different places of the substrate subjected to different deformations.

To prove the behavior of the device corresponds to an AC powder EL (ACPEL) device, data obtained from measuring at 400 and 1000 Hz of EL1 are plotted in **Figure 11** (Figure S15, Supporting Information, shows the corresponding data for EL2–EL7). Luminance is given by the following equation in ACPEL devices:[37]

$$L = L_0 \exp\left[-\left(\frac{V_0}{V}\right)^{\frac{1}{2}}\right] \quad (3)$$

where L_0 and V_0 are parameters dependent on the emissive layer characteristics (fraction of phosphor in the composite, particle size, dielectric constant of the embedding medium) and device thickness.[37] L_0 and V_0 fitting parameters, with the corresponding r^2, for EL1 at each frequency are presented in **Table 1** for thermoformed and non-thermoformed devices (for EL2–EL7, the data are provided in Table S1, Supporting Information).

It is observed that the data from EL1 are well fitted with Equation (3), meaning the mechanism of electroluminescent is the typical of ACPEL devices: injection of electrons from electrodes, tunneling of electrons from conductive Cu_xS and recombination of acceptor (Cu) and donor (Cl) on ZnS host (blue emission) or transferring of energy from the pair recombined to Mn^{2+} (yellow emission) in the host lattice.[9,37] On the other hand, the difference in L_0 and V_0 of devices before and after thermoforming may be attributed to the reduction in thickness caused by deformation. EL2–EL7 present similar values and are well fitted to Equation (3) as well.

Furthermore, the voltage threshold (V_{th}), defined as the necessary voltage to achieve 1 cd m^{-2}, was calculated as well for EL1 and it is displayed in Table 1 (Table S1, Supporting Information, for

© 2025 Wiley-VCH GmbH

2365709x, 2025, 11, Downloaded from https://advanced.onlinelibrary.wiley.com/doi/10.1002/admt.202402116 by Universidade Do Minho, Wiley Online Library on [27/04/2026]. See the Terms and Conditions (https://onlinelibrary.wiley.com/terms-and-conditions) on Wiley Online Library for rules of use; OA articles are governed by the applicable Creative Commons License

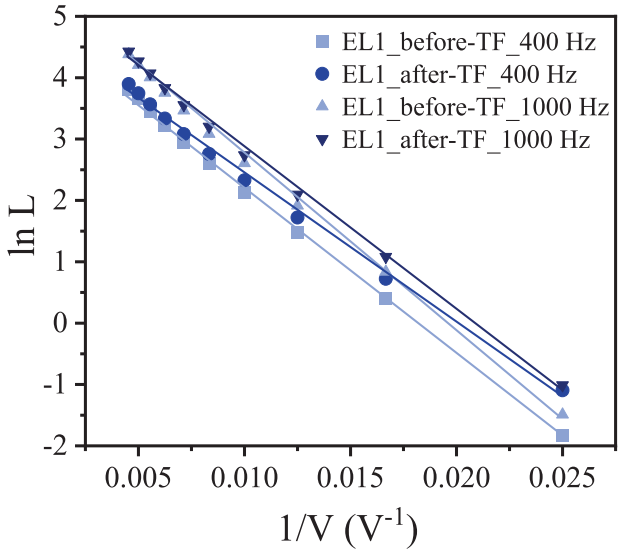


Figure 11. Linear fitting of EL1 luminescence (at different frequencies before and after thermoforming) to ACPEL behavior.

the other electrodes). Electroluminescence recorded below this voltage is only detected in absolute darkness.[38] Thus, that light emission will be lost in the noise since the device is not thought to work in absolute darkness. Values from EL2 to EL7 are very similar to EL1, as expected.

Luminous efficacy was calculated based on luminance measurements, the applied excitation voltage, and the measured electrical current consumed by the electrodes, following Equation (4).

$$\text{Luminous efficacy} = \frac{\text{L}}{V \cdot I} \tag{4}$$

where L is luminance, V is voltage, and I is the electrical current.

Figure 12 presents a) the luminous efficacy at 120 V as a function of frequency and b) the efficacy at 400 and 1000 Hz as a function of voltage, both before and after thermoforming. As shown, luminous efficacy increases with voltage but decreases with increasing frequency. Although luminance rises with frequency, the increased power consumption by the electrodes offsets this luminance gain, leading to a reduction in overall efficiency. In contrast, increasing the excitation voltage results in a simultaneous rise in both luminance and efficiency. The highest efficacy was observed at 220 V and 400 Hz.

The thermoforming process further improved efficiency across all electrodes, with an average efficacy increase of 14.8% across all tests. The maximum efficacy gain was recorded at 40 V and 1000 Hz, with an improvement of 39.3%.

The calculated efficacy for the electrodes EL2–EL7, before and after thermoforming, is collected in Figures S16–S21 (Supporting Information).

Table 1. Linear fitting parameters and coefficient of determination of EL1 at each frequency before (b-) and after (a-) thermoforming.

	b-TF_400 Hz	a-TF_400 Hz	b-TF_1000 Hz	a-TF_1000 Hz
r^2	0.9986	0.9962	0.9981	0.9972
L_0 [cd m^{-2}]	141	130	256	242
V_0 [V]	546	487	568	528
V_{th} [V]	55	50	51	48

3.4. Electroluminescent and Capacitive Interface Operation

In **Figure 13**, the combination of the capacitive touch detection and the EL response is analyzed. Due to the characteristics of the circuit, the same electrode cannot work as capacitive sensor and electroluminescent region at the same time. Thus, EL2 is connected to the capacitive reading inputs and EL1 to the electroluminescent activation channel. As it is observed, there is a clear activation of EL1 when the human finger is in the detection area of EL2. It is to notice that a switching circuit can be implemented in order to enable one electrode to work as capacitive and electroluminescent region at the same time. Alternatively, it is possible to redesign the screen-printed layers, implementing a second Ag electrode separated from the first one with another layer of dielectric, therefore, the same region will be able to work as capacitive and electroluminescent region.

Regarding stability of the prototype against thermal effects or oxidation, it is worth mentioning that the printed layers, being on the nonexposed side of the substrate, are protected by it, which provides a degree of environmental shielding. To further enhance durability and ensure prolonged use, overmolding the device with a molten polymer by injection molding can be a possibility. Thus, electrodes would be encapsulated between the substrate and the injected polymer, being protected against any change in the environment.

4. Conclusions

This work presents a new approach to electronic human-machine interface systems, based on thermoformed printed electronics and combining electroluminescent and capacitive sensing capabilities. The device was studied before and after thermoforming in terms of morphological, electrical, and electroluminescent properties. The operation of the electroluminescent and capacitive interface of the 3D device was addressed as a computer mouse prototype.

The system is composed by four screen-printed layers: PEDOT:PSS, phosphor, dielectric, and silver layer. The SEM images of the devices before and after thermoforming showed a heterogeneous distribution of electroluminescent particles in the phosphor layer but it does not seem to affect the light emission uniformity observed in the electroluminescent measurements. Ag and PEDOT:PSS layers behave different toward thermoforming as it was concluded from the resistance measurements. The process is favorable for the electrical conductivity of the former and negative for the electrical conductivity of the latter. Moreover, thermoforming allowed to complete the sintering of the Ag ink. On the other hand, impedance spectroscopy measurements indicated that the electrode stacks are able to operate at frequencies up to 2 kHz with optimum performance. Furthermore, a minor variation in dielectric performance was observed between the thermoformed

 © 2025 Wiley-VCH GmbH

2365709x, 2025, 11, Downloaded from https://advanced.onlinelibrary.wiley.com/doi/10.1002/admt.202402116 by Universidade Do Minho, Wiley Online Library on [27/04/2026]. See the Terms and Conditions (https://onlinelibrary.wiley.com/terms-and-conditions) on Wiley Online Library for rules of use; OA articles are governed by the applicable Creative Commons License

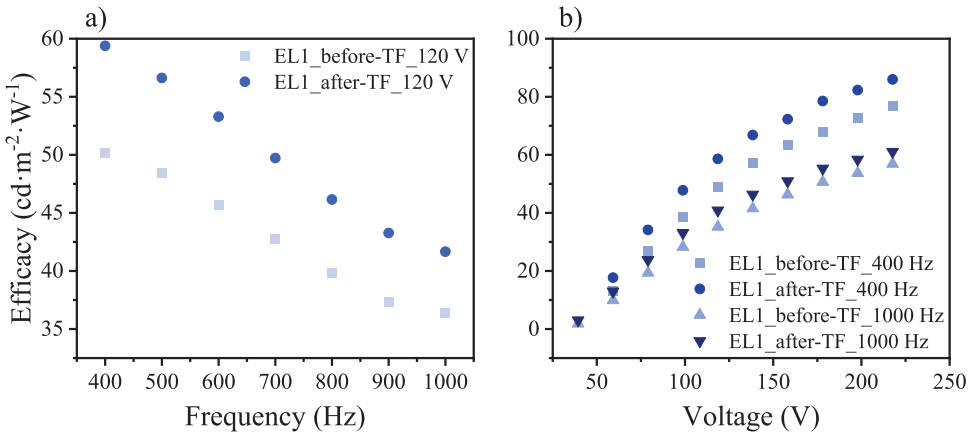


Figure 12. Luminous efficacy of EL1 at a) 120 V in function of frequency and b) 400 and 1000 Hz in function of voltage.

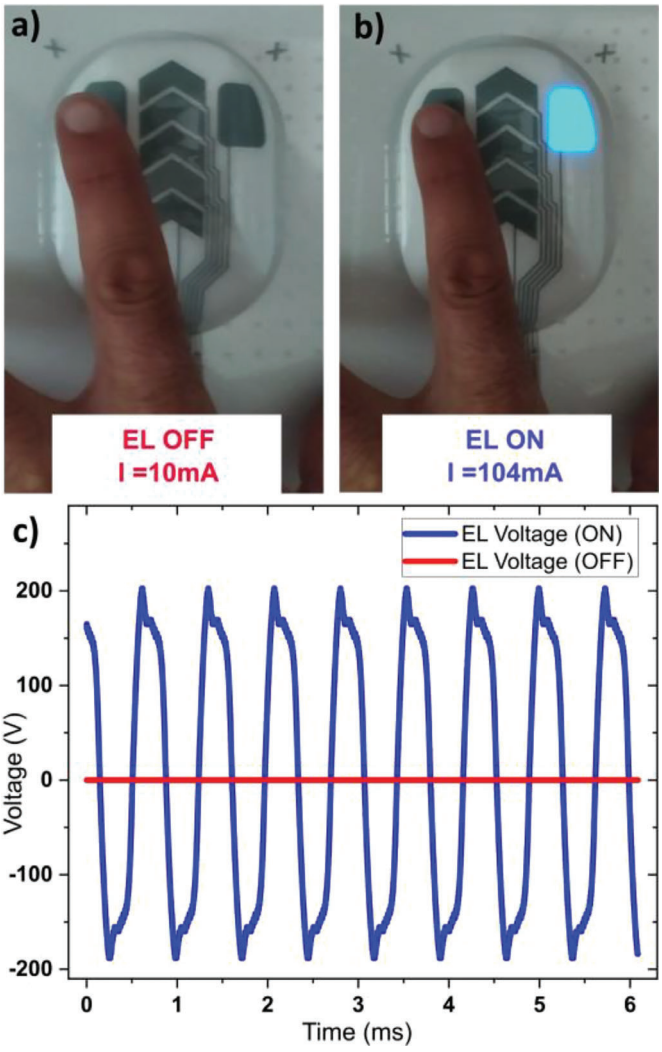


Figure 13. a) Prototype without capacitive touch detection, the electroluminescent circuit is not activated. b) Prototype with capacitive touch detection, the electroluminescent circuit is activated. c) Polarization waveform of the electroluminescent region.

and non-thermoformed devices, attributed to the completion of the sintering process of the ink. Electroluminescent characterization revealed that thermoforming improved efficacy across all electrodes, with an average increase of 14.8%. The highest luminous efficacy was observed at 220 V and 400 Hz.

Finally, the device was connected to the electronic system to verify the ability of the circuit to work as a capacitive sensor and perform a luminous actuation. Under normal visibility conditions, electrodes were able to work as capacitive sensors and electroluminescent actuators as long as each function is carried out by different electrodes. Implementing a switching circuit or more layers in the screen-printed device will enable the same region to work as sensor and actuator at the same time. Thus, the potential of IME technology as a high-deformation solution was demonstrated, highlighting its suitability for HMI applications in various sectors, ranging from car interiors to medical devices.

Supporting Information

Supporting Information is available from the Wiley Online Library or from the author.

Acknowledgements

L.C.-A. thanks the University of Basque Country (UPV/EHU) for the doctoral grant PIFI20/04 and Portuguese Foundation for Science and Technology (FCT) under strategic funding PTDC/03781/2022. This study formed part of the Advanced Materials program and was supported by MCIN with funding from European Union NextGenerationEU (PRTR-C17.I1) and the IKUR Strategy of the Department of Education of the Basque Government. Funding by the Basque Government Industry Departments under the ELKARTEK programs is also acknowledged. The authors thank the technical and human support provided by SGIker (UPV/EHU).

Conflict of Interest

The authors declare no conflict of interest.

Author Contributions

L.C.-A.: formal analysis (lead); investigation (lead); writing – original draft (lead); N.P.: conceptualization (equal); investigation (equal); supervision

© 2025 Wiley-VCH GmbH

2365709x, 2025, 11, Downloaded from https://advanced.onlinelibrary.wiley.com/doi/10.1002/admt.202402116 by Universidade Do Minho, Wiley Online Library on [27/04/2026]. See the Terms and Conditions (https://onlinelibrary.wiley.com/terms-and-conditions) on Wiley Online Library for rules of use; OA articles are governed by the applicable Creative Commons License

(lead); writing – review & editing (lead); J.V.: formal analysis (equal); investigation: (equal); writing – original draft (equal); writing – review & editing: (equal); V.M.G.C.: conceptualization (equal); formal analysis (equal); investigation (equal); writing – original draft (equal); C.M.-F.: investigation (supporting); writing – review & editing (supporting); J.L.V.-V.: funding acquisition (equal); supervision (equal); writing – review & editing (equal); S.L.-M.: conceptualization (lead); funding acquisition (lead); project administration (lead); supervision (equal); writing – review & editing (equal).

Data Availability Statement

The data that support the findings of this study are available from the corresponding author upon reasonable request.

Keywords

capacitive sensing, conformable electronics, electroluminescent, in-mold electronics, thermoforming

Received: December 12, 2024
Revised: January 27, 2025
Published online: February 19, 2025

[1] H. Zhu, X. Hu, B. Liu, Z. Chen, S. Qu, *ACS Appl. Mater. Interfaces* **2021**, *13*, 59243.
[2] M. Miliciani, G. M. Mendicino, M. T. DeMeuse, *Flexible Printed Electron.* **2023**, *8*, 035011.
[3] S. I. S. Shahabadi, J. M. R. Tan, S. Magdassi, *Coatings* **2023**, *13*, 1548.
[4] N. Hammes, C. Ribeiro, C. Machado, J. Ferreira, R. Campos, D. Faye, A. Cortez, S. Melo, F. Duarte, A. Pontes, J. C. Viana, P. Pedrosa, N. Homem, *Flexible Printed Electron.* **2023**, *8*, 025022.
[5] O. Rusanen, T. Simula, P. Niskala, V. Lindholm, M. Heikkinen, in *2019 22nd European Microelectronics Packaging Conf. Exhibition (EMPC)*, IEEE, Piscataway, NJ **2019**, pp. 1–7.
[6] A. Wimmer, H. Reichel, K. Schmidt, in *2018 13th Int. Congress Molded Interconnect Devices (MID)*, IEEE, Piscataway, NJ **2018**, pp. 1–5.
[7] J. Wang, M.-F. Lin, S. Park, P. S. Lee, *Mater. Today* **2018**, *21*, 508.
[8] L. Tenchine, O. Dassonville, in *2016 12th Int. Congress Molded Interconnect Devices (MID)*, IEEE, Piscataway, NJ **2016**, pp. 1–6.
[9] K. W. Park, H. S. Jeong, J. H. Park, G. Deressa, Y. T. Jeong, K. T. Lim, J. H. Park, S. H. Lee, J. S. Kim, *J. Lumin.* **2015**, *165*, 216.
[10] Y. Lin, W. Yuan, C. Ding, S. Chen, W. Su, H. Hu, Z. Cui, F. Li, *ACS Appl. Mater. Interfaces* **2020**, *12*, 24074.
[11] M. Beltrão, F. M. Duarte, J. C. Viana, V. Paulo, *Polym. Eng. Sci.* **2022**, *62*, 967.
[12] *IDTechEx, "IDTechEx Research: In-Mold Electronics 2020–2030: Technology, Market Forecasts, Players"*, **2019**, https://www.idtechex.com/en/research-report/in-mold-electronics-2020-2030-technology-market-forecasts-players/722 (accessed October 2024).
[13] K. Wu, Q. Zhou, H. Zou, K. Leng, Y. Zeng, Z. Wu, *Micromachines* **2019**, *10*, 160.
[14] J. Schirmer, M. Reichenberger, A. Wimmer, H. Reichel, S. Neermann, J. Franke, in *2021 14th Int. Congress: Molded Interconnect Devices, MID 2021 – Proceedings*, Institute of Electrical and Electronics Engineers, Amberg, Germany **2021**.
[15] S.-C. Chen, H.-M. Li, S.-T. Huang, Y.-C. Wang, *Int. Commun. Heat Mass Transfer* **2010**, *37*, 501.
[16] J. C. Hess, *Chip Production's Ecological Footprint: Mapping Climate and Environmental Impact*, Interface, Berlin, Germany **2024**.
[17] M. Bakr, F. Bossuyt, J. Vanfleteren, *Flexible Printed Electron.* **2022**, *7*, 023001.
[18] X. Gong, K. Huang, Y.-H. Wu, X.-S. Zhang, *Sens. Actuators, A* **2022**, *345*, 113821.
[19] Y. Zhang, Y. Zhu, S. Zheng, L. Zhang, X. Shi, J. He, X. Chou, Z.-S. Wu, *J. Energy Chem.* **2021**, *63*, 498.
[20] P. J. Martin, *Advances in Polymer Processing*, Elsevier, Amsterdam **2009**, pp. 352–383.
[21] S. Y. Lee, S. H. Jang, H. K. Lee, J. S. Kim, S. Lee, H. J. Song, J. W. Jung, E. S. Yoo, J. Choi, *Org. Electron.* **2020**, *85*, 105881.
[22] S. Zulfiqar, A. A. Saad, M. F. M. Sharif, Z. Samsudin, M. Y. T. Ali, F. C. Ani, Z. Ahmad, M. K. Abdullah, *Microelectron. Reliab.* **2021**, *127*, 114373.
[23] G. Destriau, *J. Chim. Phys.* **1936**, *33*, 587.
[24] W. A. D. M. Jayathilaka, A. Chinnappan, J. N. Tey, J. Wei, S. Ramakrishna, *J. Mater. Chem. C* **2019**, *7*, 5553.
[25] F. Ma, Y. Lin, W. Yuan, C. Ding, W. Su, X. Meng, Z. Cui, *ACS Appl. Electron. Mater.* **2021**, *3*, 1747.
[26] M. M. Afandi, J. Kim, *J. Lumin.* **2024**, *265*, 120201.
[27] R. Polícia, N. Peřinka, C. Mendes-Felipe, P. Martins, D. M. Correia, S. Lanceros-Méndez, *Adv. Sustainable Syst.* **2024**, *8*, 2400140.
[28] Z. Yang, W. Wang, J. Pan, C. Ye, *Cell Rep. Phys. Sci.* **2020**, *1*, 100213.
[29] D. H. Smith, *J. Lumin.* **1981**, *23*, 209.
[30] M. Gill, A. Gruner, N. Ghalib, M. Sussman, S. Avuthu, G. Wable, J. Richstein, in *IPC APEX EXPO Proc*, St. Petersburg, Florida, USA **2018**.
[31] X. Liu, D. Li, H. Fukutani, P. Trudeau, L. Khoun, O. Mozenson, K. L. Sampson, M. Gallerneault, C. Paquet, T. Lacelle, B. Deore, O. Ferrand, J. Ferrigno, P. R. L. Malenfant, A. J. Kell, *Adv. Electron. Mater.* **2021**, *7*, 2100194.
[32] Y. A. Ono, *Electroluminescent Displays*, World Scientific, Singapore **1995**.
[33] J. Liao, J. Sun, F. Dong, Y. Chang, S. Chang, X. Mao, N. Li, X. Li, Y. Wang, Y. Shang, B. Wang, C. Shan, L. Dong, *Nano Energy* **2023**, *112*, 108488.
[34] B. Allieri, S. Peruzzi, L. Antonini, A. Speghini, M. Bettinelli, D. Consolini, G. Dotti, L. E. Depero, *J. Alloys Compd.* **2002**, *341*, 79.
[35] C. K. Rastogi, R. K. Mishra, S. Chirauri, K. R. Rao, R. K. Vatsa, R. M. Kadam, V. Sudarsan, *Physica B: Condens. Matter* **2022**, *640*, 414054.
[36] J. H. Park, S. H. Lee, J. S. Kim, A. K. Kwon, H. L. Park, S. D. Han, *J. Lumin.* **2007**, *126*, 566.
[37] X. Zhang, F. Wang, *APL Mater.* **2021**, *9*, 030701.
[38] P. Harris, D. den Engelsen, G. Fern, J. Silver, *J. Mater. Sci.: Mater. Electron.* **2017**, *28*, 7006.

© 2025 Wiley-VCH GmbH

2365709x, 2025, 11, Downloaded from https://advanced.onlinelibrary.wiley.com/doi/10.1002/admt.202402116 by Universidade Do Minho, Wiley Online Library on [27/04/2026]. See the Terms and Conditions (https://onlinelibrary.wiley.com/terms-and-conditions) on Wiley Online Library for rules of use; OA articles are governed by the applicable Creative Commons License